Pergamon

Int. J. Heat Mass Transfer. Vol. 40, No. 11, pp. 2647–2653, 1997

Printed in Great Britain
0017–9310/97 $17.00+0.00

PII: S0017-9310(96)00263-3

Numerical study of recovery effect and impingement heat transfer with submerged circular jets of large Prandtl number liquid

X. C. LEE, C. F. MA,† Q. ZHENG, Y. ZHUANG and Y. Q. TIAN

Department of Thermal Science and Engineering, Beijing Polytechnic University, Beijing 100022, China

(*Received* 1 *August* 1996)

Abstract—A numerical study was conducted to characterize the thermal behavior of laminar circular liquid jets. The main goal of this work was to clarify the significant recovery effect of large Prandtl number liquid jets reported by the present authors. Radial distribution of local recovery factor was studied in numerical detail. The effects of many factors were investigated including Reynolds number, Prandtl number, nozzle-to-plate spacing, jet velocity, nozzle diameter and velocity profile at nozzle exit. Very large recovery factors over 20 were obtained with high Prandtl number fluid jets at medium velocity. The results exhibited good agreement with the experimental data by the present authors, verifying the great significance of recovery effect with large Prandtl number liquid jets.

1. INTRODUCTION

Impinging fluid jets can provide very high heat and mass transfer rates, particularly with liquid as the working medium [1]. As an attractive cooling option, liquid jet impingement has been employed in many technical processes. Some industrial applications include cooling of internal combustion engines [2], thermal treatment of metals [3] and, more recently, thermal control of electronic devices [4].

It has been established that the difference between the wall temperature and the adiabatic wall (or recovery) temperature is the thermal driving force for impinging high speed air jets [5–7] or large Prandtl number liquid jets at medium velocity [8–11]. In consequence, the heat transfer coefficient h should be defined as

$$h = \frac{q}{t_w - t_{aw}} \tag{1}$$

where the adiabatic wall temperature T_{aw} is calculated from

$$t_{aw} = t_0 + r\frac{\bar{u}_0^2}{2C_p}. \tag{2}$$

The local characteristics of impingement heat transfer coefficient and recovery factor have been studied with circular transformer oil jets in experiment detail [8, 10]. Very large recovery factor up to 20 was reported at jet velocity about 20 m s^{-1}. Complex radial distribution of the recovery factor was recorded with a local minimum at stagnation point and two symmetric maxima on each side at $r/d \approx \pm 1.2$. It is hoped that these experimental results from Refs. [8–10] may be further clarified by numerical study. However, to the best knowledge of the present authors, numerical investigations for submerged jets were reported only for air jets [12–14] in open literature.

The objective of this work was to conduct a numerical study to characterize the recovery effect and heat transfer process with submerged impinging liquid jets with Prandtl number between 10 and 1000. The emphasis was placed on the investigation of local recovery factor. Some results of recovery factor were compared with the experimental data obtained in Ref. [10]. In general, the agreement between the numerical and experimental results was pretty good. Based on the dissipation function [15–17], interpretation was presented for the results obtained in this study. The influence of recovery effect on impingement heat transfer was also explored in this study.

2. MATHEMATICAL FORMULATION AND NUMERICAL PROCEDURE

The flow geometry and solution domain to be considered are shown in Fig. 1. A laminar jet issues from a circular tube of diameter d and impinges perpendicularly onto a flat solid surface. The submerged jet is injected directly into a miscible atmosphere. The impinging jet flows in a region bounded by the target surface and nozzle plate as shown in the figure. In the present mathematical model, the flow is assumed to be laminar, steady and axisymmetric. The effect of gravity is neglected. After non-dimensionalization, the governing equations for the control volume are expressed as follows:

† Author to whom correspondence should be addressed.

NOMENCLATURE

C_p	specific heat at constant pressure
d	nozzle diameter
Ec	$\bar{u}_0^2/(C_p \cdot t_0)$, non-dimensional group
h	heat transfer coefficient
K	empirical constant in equation (6)
k	thermal conductivity
Nu	$h \cdot d/k$, Nusselt number
P	$p/(\rho \cdot u_0^2)$m, non-dimensional static pressure
p	static pressure
Pr	v/α, Prandtl number
Q	$q/\rho C_p \bar{u}_0 t_0$, non-dimensional heat flux
q	heat flux
R	radial coordinate
R^*	R/d, non-dimensional radial coordinate
r	recovery factor
Ra^*	$(\sqrt{(320/K)-95}-7)/16$ [empirical constant]
Re	$u_0 \cdot d/v_0$, Reynolds number
T	$(t-t_0)/t_0$, non-dimensional static temperature
t	static temperature
t_{aw}	adiabatic wall temperature
t_w	wall temperature
t_0	the jet static temperature at nozzle exit
U	$u/\bar{u}_0$, non-dimensional radial velocity
u	radial velocity component
$\bar{u}_0$	mean jet velocity at nozzle exit
V	$v/\bar{u}_0$, non-dimensional axial velocity component
v	axial velocity component
X	x/d, non-dimensional coordinate normal to impingement plate
x	coordinate normal to impingement plate
z	nozzle-to-plate spacing.

Greek letters

μ	dynamic viscosity
α	thermal diffusivity
ν	kinematic viscosity
ν^*	ν/ν_0, non-dimensional kinematic viscosity
ρ	density
Φ	dissipation function.

Superscripts and subscripts

—	average values.
0	variables at the nozzle exit
max	maximum value.

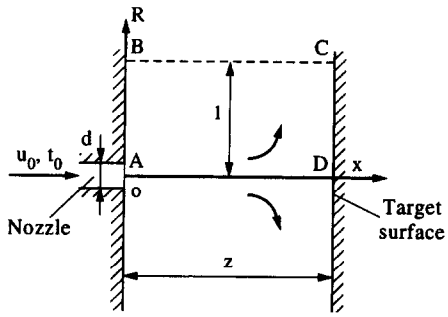

Fig. 1. Physical model and coordinate system.

The continuity equation

$$\frac{\partial U}{\partial X}+\frac{1}{R^*}\frac{\partial R^*V}{\partial R^*}=0. \tag{3}$$

The momentum equations

$$U\frac{\partial U}{\partial X}+V\frac{\partial U}{\partial R^*}=\frac{1}{Re}\left[\frac{\partial}{\partial X}\left(\nu^*\frac{\partial U}{\partial X}\right)+\frac{1}{R^*}\frac{\partial}{\partial R^*}\left(R^*\nu^*\frac{\partial U}{\partial R^*}\right)\right]-\frac{\partial P}{\partial X}+\frac{1}{Re}\left[\frac{\partial}{\partial X}\left(\nu^*\frac{\partial U}{\partial X}\right)+\frac{1}{R^*}\frac{\partial}{\partial R^*}\left(R^*\nu^*\frac{\partial V}{\partial X}\right)\right]$$

$$U\frac{\partial V}{\partial X}+V\frac{\partial V}{\partial R^*}=\frac{1}{Re}\left[\frac{\partial}{\partial X}\left(\nu^*\frac{\partial V}{\partial X}\right)+\frac{\partial}{\partial R^*}\left(\frac{\nu^*}{R^*}\frac{\partial R^*V}{\partial R^*}\right)\right]-\frac{\partial P}{\partial R^*}+\frac{1}{Re}\left[\frac{\partial}{\partial X}\left(\nu^*\frac{\partial U}{\partial R^*}\right)+\frac{\partial}{\partial R^*}\left(\frac{\nu^*}{R^*}\frac{\partial R^*V}{\partial R^*}\right)\right]. \tag{4}$$

The energy equation

$$U\frac{\partial T}{\partial X}+V\frac{\partial T}{\partial R^*}=\frac{1}{PrRe}\left[\frac{\partial^2 T}{\partial X^2}+\frac{1}{R^*}\frac{\partial}{\partial R^*}\left(R^*\frac{\partial T}{\partial R^*}\right)\right]+\frac{Ec}{Re}\times\nu^*\left\{2\left[\left(\frac{\partial U}{\partial X}\right)^2+\left(\frac{\partial V}{\partial R^*}\right)^2+\left(\frac{V}{R^*}\right)^2\right]+\left(\frac{\partial U}{\partial R^*}+\frac{\partial V}{\partial X}\right)^2\right\}. \tag{5}$$

The solution domain is described as OABCDO in Fig. 1 with a radius of $15d$. The boundary conditions are given as follows:

$OA: T=0, V=0$

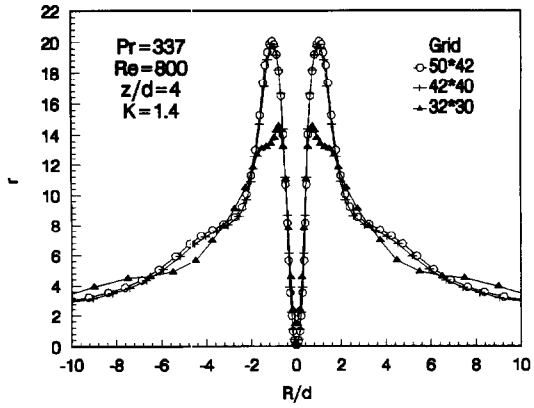

Fig. 2. The influence of the grid number.

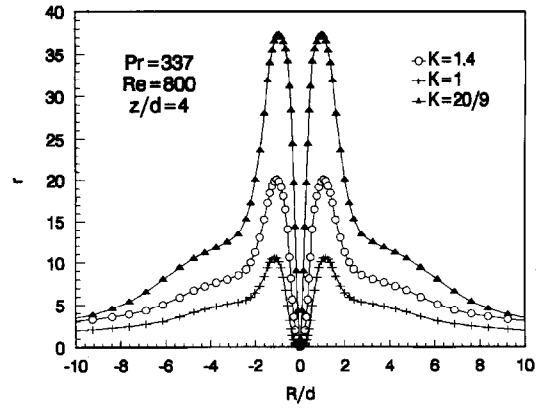

Fig. 3. Local recovery factor distributions with different jet velocity profiles.

$$U=\begin{cases} K & \text{for } R^* \leqslant Ra^* \\ K\left[1-1.5\left(\dfrac{R^*-Ra^*}{0.5-Ra^*}\right)^2\right. & \\ \left.\quad +0.5\left(\dfrac{R^*-Ra^*}{0.5-Ra^*}\right)^3\right] & \text{for } R^*>Ra^* \end{cases} \tag{6}$$

where $Ra^*=(\sqrt{(320/K)-95}-7)/16$ and K is a constant between 1 and 20/9. Apparently, $K=1$ corresponds to uniform velocity profile at the nozzle exit and $K=20/9$ corresponds to fully developed velocity profile. Between the two critical conditions the velocity profiles can be considered as semi-developed. In this work $K=1.4$ was taken in the calculation.

$$AB: \frac{\partial T}{\partial X}=0, \quad U=V=0$$

$$BC: T=0 (V<0) \text{ or } \frac{\partial T}{\partial R^*}=0 (V>0),$$

$$U=0, \quad \frac{\partial R^* V}{\partial R^*}=0$$

$$CD: \frac{\partial T}{\partial X}=PrReQ, \quad U=V=0$$

$$DO: \frac{\partial T}{\partial R^*}=0, \quad \frac{\partial U}{\partial R^*}=0, \quad V=0.$$

The equations listed above were solved with SIMPLE method. The computations were carried out with a non-uniform 50×42 staggered grid system which was good enough to obtain accurate results in this work. Figure 2 demonstrates the influence of the grid number. It is seen from the figure that the computational result is insensitive to the grid number when the number is big. As shown in the figure, the computational data are identical for the 50×42 and 42×40 grid systems. Under-relaxation factors were employed to ensure the convergence of the numerical solutions. The criterion for convergence was adopted that the relative errors for each variable between two successive iterations were less than a small value: 10^{-6} for T and 10^{-5} for U and V, respectively. Using the transformer oil as working fluid, the basic parameters in the present calculation are specified as follows:

$$\overline{u_0}=20\,\text{m s}^{-1}, d=1\,\text{mm}, t_0=30^\circ C,$$

$$\rho=860\,\text{kg m}^{-3}, C_p=1943\,\text{J kg K}^{-1},$$

$$\nu_0=25\times10^{-5}\,\text{m}^2\,\text{s}^{-1}, z/d=4$$

and $Pr=337, Re=800.$

In some cases, the parameters were changed in the following ranges:

$\overline{u_0}$ 10–40 m s^{-1}; d 1–1.5 mm; Pr 10–1000; z/d 2–20.

The physical properties of working fluid were assumed to be constant in this study expect for the cases of computing the recovery factor and heat transfer coefficient for comparison with the experimental data in next section paragraph 3.5, in which the viscosity and Prandtl number were considered as functions of temperature.

3. NUMERAL RESULTS AND DISCUSSION

The computational work was performed using the basic parameters presented in the foregoing unless pointed out specially. The main body of the numerical results is related to recovery factors.

3.1. *The general feature and influence of velocity profile*

It was found that the recovery factor was significantly affected by the velocity profile at the nozzle exit. As shown in Fig. 3 the fully developed profile resulted in much higher recovery factors than those with uniform profile. The former may be three times larger than the later. However, the two radial distribution curves demonstrate similar shape: a valley appears at the stagnation point and two symmetric peaks exist at around $R/d=\pm1.2$. This result is consistent with the experimental data reported in Refs. [9, 10]. In the present work a semi-developed velocity

profile ($K = 1.4$) was adopted resulting in a radial distribution of recovery factor between the two critical cases as exhibited in Fig. 3. The general feature of recovery factor associated with high Prandtl number liquid jets can be explained by means of dissipation function [15]. The dissipation function, defined and described in some classical works [16, 17], indicates the energy dissipated into heat by friction. In the present case the dimensional dissipation function can be expressed by

$$\Phi = \mu \cdot \left\{2 \cdot \left[\left(\frac{\partial u}{\partial x}\right)^2 + \left(\frac{\partial v}{\partial R}\right)^2 + \left(\frac{v}{R}\right)^2\right] + \left(\frac{\partial u}{\partial R} + \frac{\partial v}{\partial x}\right)^2\right\}.$$

It has been included in the second term on the right-hand-side of equation (5). At stagnation point we certainly have $\partial u/\partial R = \partial v/\partial R = 0$ because of velocity profile symmetry and $v = 0$ because of velocity stagnation. Also, we can assume $\partial u/\partial x = \partial v/\partial x = 0$ at the stagnation point on the wall. In consequence, the dissipation function becomes zero at stagnation point. It means that the wall temperature increase, owing to frictional heat, is zero or the recovery factor is zero at this point. In contrast to the circumstance at stagnation point, very large velocity gradient appears in the vicinity of this point, resulting in a large dissipation function. For large Prandtl number liquid jets, the dissipation function is even greater in this area because of the large magnitude of dynamic viscosity. So, large recovery factors exist around the stagnation point as shown in Fig. 3. The large difference in recovery factors between uniform and fully developed velocity profiles can also be explained by the variation of dissipation function. In reality, the parabolic velocity profile yields a much greater value of velocity gradient than uniform velocity jets. As a result, a larger dissipation function or recovery factor can be obtained. More detailed information about the relationship between the recovery factor and dissipation function is reported in Ref. [15].

3.2. *Effect of Reynolds number*

Numerical study was conducted to investigate the effect of Reynolds number. The result is presented in Fig. 4. It is observed that the recovery factor distribution is very slightly affected by Reynolds number. This trend is in agreement with the experimental results both of impinging liquid [9, 10] and air [7] circular jets. The effect of varying nozzle diameter or jet velocity was also studied under constant Reynolds numbers. As shown in Fig. 5, the effect can be neglected in the range of the parameters investigated in the present work.

3.3. *Influence of Prandtl number*

Significant influence of Prandtl number on recovery factor was determined in this study. Fig. 6 presents the radial distributions of recovery factor for constant Prandtl numbers between 10 and 1000. The distribution curves display the same contour, but they

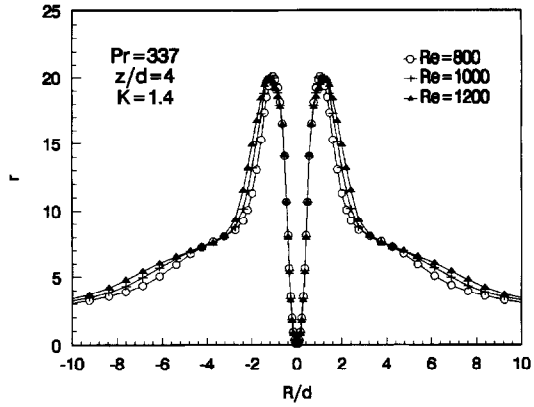

Fig. 4. Local recovery factor distributions for various jet Reynolds numbers.

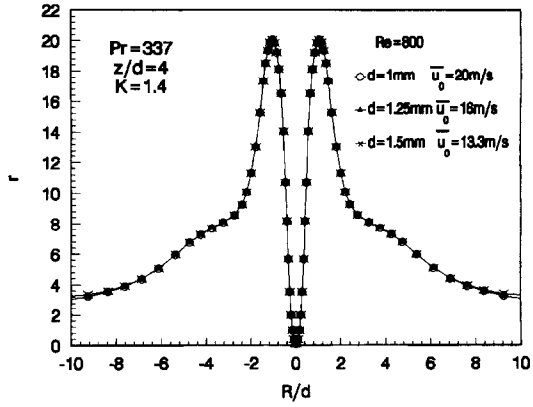

Fig. 5. Local recovery factor distributions for various nozzle diameters.

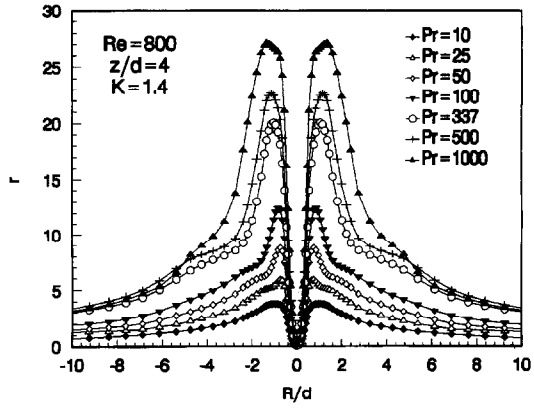

Fig. 6. Local recovery factor distributions at various Prandtl numbers.

are very different in magnitude. It is seen from the figure that recovery factors increase significantly with increasing Prandtl number. The peak value of the recovery factor can be correlated as a function of Prandtl number by the following equations:

$$r_{max} = 1.20\,Pr^{0.5} \quad \text{for } 10 < Pr < 200 \qquad (7)$$

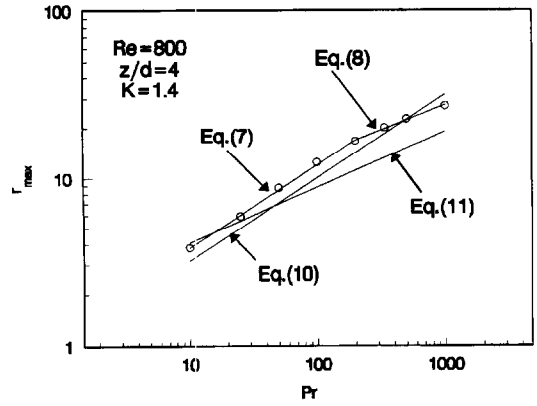

Fig. 7. Variation of maximum recovery factor with Prandtl number.

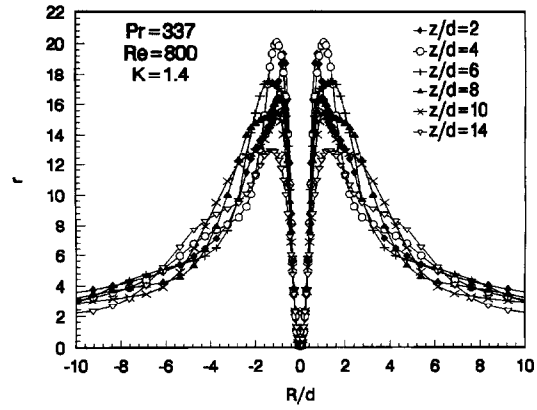

Fig. 8. Local recovery factor distributions at various nozzle-to-plate spacings.

$$r_{max} = 3.46\,Pr^{0.3} \quad \text{for } 200 < Pr < 1000. \tag{8}$$

Equations (7) and (8) are within ± 3 and $\pm 1.5\%$ of the correspondent numerical data, respectively. A single correlation was also developed for all the data over the entire range of Prandtl number from 10 to 1000:

$$r_{max} = 1.51\,Pr^{0.437} \quad \text{for } 10 < Pr < 1000. \tag{9}$$

This correlation presents all the data within $\pm 14\%$. Very good agreement is seen from Fig. 7 between the numerical data and the predicted curves by equations (7) and (8). Presented in the figure are also the two correlations developed both for laminar flow along a flat plate [16, 17]:

$$r = \sqrt{Pr} \tag{10}$$

$$r = 1.9 \cdot Pr^{1/3}. \tag{11}$$

Equation (10) was reported to be a good approximation for parallel flow with Prandtl number between 0.6 and 15 [16]. Equation (11) was proposed for large Prandtl number between 100 and 1000 [17]. As shown in Fig. 7, the two correlations, particularly the former, may be used as a first approximation to estimate the maximum recovery factor associated with impinging jets of large Prandtl number fluid.

Prandtl number may vary from liquid to liquid by several orders of magnitude. The Prandtl number is the ratio of kinematic viscosity and the thermal diffusion. Large Prandtl number is associated with greater magnitude of dynamic viscosity μ, or greater dissipation function. Consequently, a larger amount of heat generated by friction can be obtained with higher Prandtl number. On the other hand, larger Prandtl number should indicate smaller rates at which heat may diffuse through the fluid, resulting in less loss of frictional heat. The above discussion provides the interpretation for the relationship between recovery factor and Prandtl number illustrated in Figs. 6 and 7.

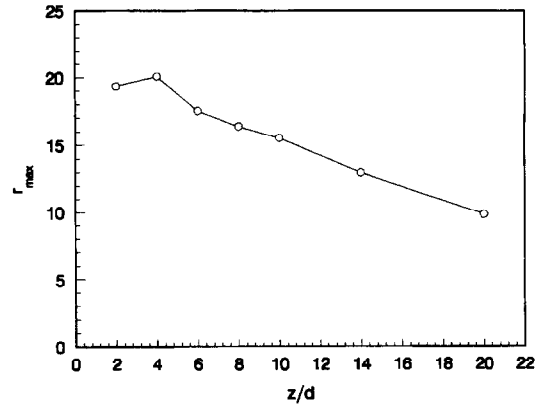

Fig. 9. Variation of maximum recovery factor with nozzle-to-plate spacing.

3.4. *Effect of nozzle-to-plate spacing*

Seven distribution curves of recovery factor are plotted in Fig. 8 for corresponding constant z/d. In general, the variation of nozzle-to-plate spacing does not change the curve shape. However, the maximum r_{max} is affected by the spacing. Non-monotonous variation of r_{max} with z/d is exhibited in Fig. 9 with a maximal value at $z/d = 4$. Beyond this peak the recovery factor decreases with the increase of spacing.

3.5. *The influence of recovery effect on heat transfer*

In Fig. 10 two radial distributions of local heat transfer coefficients are presented at constant heat flux $q = 10^5$ w m^{-2}, corresponding to the cases with recovery effect included and neglected, respectively. Apparently, the local Nusselt numbers calculated from recovery temperature are somewhat higher than those with recovery effect neglected, particularly in the stagnation zone ($R/d < 2$). It is noted that a significant valley appears at the stagnation point resulted from the recovery effect. Beyond $R/d = 3$ the difference between the two curves can be neglected.

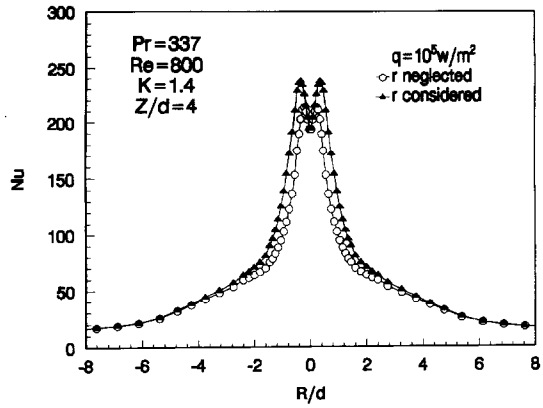

Fig. 10. Local heat transfer distributions with and without recovery effect.

3.6. *Comparison with experimental data*

In order to make a comparison with the experimental data from Ref. [10], numerical work was performed using the parameters identical with those in the reference: $\overline{u_0} = 23.2$ m s^{-1}, $d = 0.987$ mm, $t_0 = 37.5°C$, $Pr = 263$, $v_0 = 19.08 \times 10^{-6}$ m^2 s^{-1} and $z/d = 4$ or 8. The comparison of the numerical result with the experimental data is demonstrated in Fig. 11. In general, the agreement is pretty good between the computed curves and the experimental data. At the stagnation point the experimental data are much higher than zero value by the calculation. It can be attributed to the fact that the measured wall temperature in Ref. [10] is not exactly a local value, but an average one over a small range due to the definite size (∅0.8 mm) of the thermocouples and the lateral thermal conduction along the metal foil. The discrepancy between the numerical and experimental data is also caused by the difference in jet configurations. In the presented work confined jets are considered which are different from the unconfined jets in Ref. [10]. The agreement shown in the figure should further clarify and confirm the local characteristics of recovery factor revealed by the present authors [8–10].

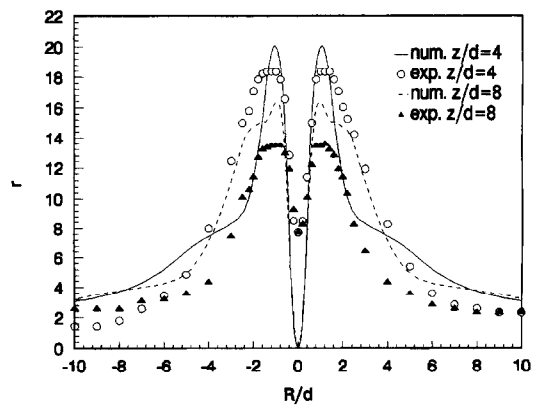

Fig. 11. Comparison of numerical result with experimental data.

4. CONCLUSIONS

A mathematical model for evaluating the thermal behavior of laminar circular impinging liquid jets was constructed. Numerical investigation was conducted with emphasis on the recovery effect with large Prandtl number liquid jets. Radial distribution of the local recovery factor was determined with the variation of Reynolds and Prandtl numbers. The influence of jet velocity profile at nozzle exit and nozzle-to-plate spacing was also examined numerically. The results confirmed the great importance of recovery effect in the thermal process with impinging large Prandtl number liquid jets. Good agreement between the present results and available experimental data was observed. The general characteristics of recovery factor revealed in this work were interpreted by means of dissipation function.

Acknowledgements—Support of this work from National Natural Science Foundation of China is gratefully acknowledged. The authors also highly appreciate Professors S. Y. Ko, W. Q. Tao and Z. Y. Guo for their valuable suggestions.

REFERENCES

1. Webb, B. W. and Ma, C.-F., Single phase liquid jet impingement heat transfer. *Advance in Heat Transfer*, 1995, **26,** 105–217.
2. Kiryu, M., Development of oil-cooled 750 cc motorcycle engine. *Automobile Technology*, 1986, **40,** 1154–1158 (in Japanese).
3. Kohing, F. C., Waterwall: water cooling systems. *Iron–Steel Engineer*, 1985, **62,** 30–36.
4. Raneko, A., Seyama, K. and Suzuki, M., LSI Packaging and cooling technologics for Fujitsu VP2000 Series. *FUJITSU*, 1990, **41(1),** 12.
5. Gardon, R. and Cobonpue, J., Heat transfer between a flat plate and jets of air impinging on it. *Proceeding of 2nd International Heat Transfer Conference*, 1962, pp. 454–460.
6. Sparrow, E. M., Goldstein, R. J. and Rouf, M. A., Effect of nozzle-surface separation distance on impingement heat transfer for a jet in a crossflow. *ASME Journal of Heat Transfer*, 1975, **97,** 528–533.
7. Goldstein, R. J., Behbahani, A. I. and Kieger Heppelmann, K., Streamwise distribution of the recovery factor and the local heat transfer coefficient to an impinging jet. *International Journal Heat Mass Transfer*, 1986, **112,** 1227–1235.
8. Ma, C.-F., Sun, H., Auracher, H. and Gomi, T., Local convective heat transfer from vertical heated surfaces to impinging circular jets of large Prandtl number fluid. *The 9th International Heat Transfer Conference*, 1990, Vol. 2, pp. 441–446.
9. Lee, X. C., Ma, C. F., Zhuang, Y. and Zheng, Q., Experimental research on recovery effect of liquid circular jet impingement, *Proceedings of the 3rd International Symposium on Multiphase Flow and Heat Transfer*, Xian, China, 1994, pp. 456–463.
10. Ma, C. F., Zheng, Q., Lee, S. C. and Gomi, T., Impingement heat transfer and recovery effect with submerged jets of large Prandtl number liquid—I. Unconfined circular jets, *International Journal of Heat and Mass Transfer*, 1997, **40,** 1481–1490.
11. Metzger, D. E., Cummings, K. N. and Ruby, W. A., Effects of Prandtl number on heat transfer characteristics of impinging liquid jets, *Proceedings of the 5th Inter-*

national Heat Transfer Conference, Hemisphere, 1974, Vol. 2, pp. 20–24.
12. Al-Sanea, Sami, A numerical study of the flow and heat transfer characteristics of an impinging laminar slot-jet including crossflow effects, *International Journal of Heat and Mass Transfer*, 1992, **35**(10) 2501–2513.
13. Kim, Joo-Kyun and Aihara, Toshio, A numerical study of heat transfer due to an axisymmetric laminar impinging jet of supercritical carbon dioxide. *International Journal of Heat and Mass Transfer*, 1992, **35**(10), 2515–2526.
14. Li, P. W. and Tao, W. Q., Numerical and experimental investigation on heat/mass transfer of slot-jet impingement in a rectangular cavity. *International Journal of Heat and Fluid Flow*, 1993, **14**, 246–253.
15. Li, D. Y., Guo, Z. Y. and Ma, C. F., Relationship between recovery factor and viscous dissipation in a confined impinging circular jet of high Prandtl number liquid (Submitted).
16. Eckert, E. R. G. and Drake, R. M., *Analysis of Heat and Mass Transfer*. McGraw-Hill, New York, 1972, Chapter 6, pp. 254–280 and chapter 10, pp. 417–438.
17. Schlichting, H., *Boundary Layer Theory*. McGraw-Hill, New York, 1979, chapter 12, pp. 265–326.